Balloon flight demonstration of coronagraph focal plane wavefront correction with PICTURE-C

Christopher B. Mendillo,* **Kuravi Hewawasam, Jason Martel** ,
Thaddeus Potter, Timothy A. Cook , **and Supriya Chakrabarti**
University of Massachusetts Lowell, Lowell Center for Space Science and Technology,
Lowell, Massachusetts, United States

Abstract. The Planetary Imaging Concept Testbed Using a Recoverable Experiment - Coronagraph (PICTURE-C) mission is designed to directly image debris disks and exozodiacal dust around nearby stars from a high-altitude balloon using a 60 cm diameter off-axis telescope and a vector vortex coronagraph. During its second flight from Fort Sumner, New Mexico, on September 28, 2022, PICTURE-C successfully used its high and low-order wavefront control systems to perform focal plane wavefront correction for the first time on an observatory in a near-space environment. The coronagraph achieved a modest broadband (20%) contrast of 5×10^{-6}, with performance limited by dynamic pointing transients. The low-order wavefront control system achieved optical pointing stabilization of 1 milliarcseconds (mas) root mean squared (RMS) over 30 second timescales. © *The Authors. Published by SPIE under a Creative Commons Attribution 4.0 International License. Distribution or reproduction of this work in whole or in part requires full attribution of the original publication, including its DOI.* [DOI: 10.1117/1.JATIS.9.2.025005]

1 Introduction

The Planetary Imaging Concept Testbed Using a Recoverable Experiment - Coronagraph (PICTURE-C) mission is a balloon-borne experiment designed to directly image debris-disks and exozodiacal dust around nearby stars in reflected visible light (540–660 nm).[1–5] A primary goal of the mission is to mature key technologies required to directly image exoplanets from space. The mission was designed and built at the UMass Lowell Center for Space Science and Technology (LoCSST). To achieve the high levels of starlight suppression (contrast) necessary to detect faint exoplanetary signals, PICTURE-C uses a vector vortex coronagraph (VVC) coupled with a 60 cm diameter off-axis telescope (Fig. 1). The contrast ratio is increased further by employing adaptive optics (deformable mirrors driven by several wavefront sensors) to both stabilize the stellar wavefront at high speed and perform high-precision focal plane wavefront correction using the electric field conjugation (EFC) technique.[6,7] The contrast achieved in flight depends both on the dynamic errors in the system as well as the static errors in the optics themselves. Dynamic errors caused by pointing jitter, mechanical flexing and thermal deformation have been discussed in a previous article describing the low-order wavefront sensor (LOWFS) chosen for the mission.[4] The static errors, including polarization aberration, were also analyzed previously.[3,8] The optical system is designed to achieve an in-flight contrast of 1×10^{-7} or better, which is required to detect exozodiacal dust and debris around nearby stars.

PICTURE-C performed its first flight on September 28, 2019,[2] and validated many of the technologies and sub-systems required to meet the science goals of the mission. These included: thermal monitoring and control using over 80 temperature sensors and 16 heaters, on-sky target acquisition using the Wallops Arc Second Pointer (WASP)[9] pointing system, automatic telescope alignment using a hexapod-actuated secondary mirror, and high-speed low-order wavefront control (LOWFC). A charge 4 VVC and a 5-band spectral imaging camera were also demonstrated

*Address all correspondence to Christopher B. Mendillo, christopher_mendillo@uml.edu

during the 2019 flight. These were replaced by a charge 6 VVC and a single wide-band imaging system (540–660 nm) for the second flight.[2] The charge 6 VVC is more tolerant to low-order aberrations[10] and the simplified imaging system reduces scattered light and produces higher signal-to-noise ratio (SNR) images.

The second flight of PICTURE-C was attempted first in 2021 from Fort Sumner, but three straight weeks of inclement weather (strong surface and upper-level winds) prevented the mission from launching. The payload was returned to UMass Lowell for eight months of continued development[1] and returned to Fort Sumner in August 2022. The mission was successfully launched on September 28, 2022, three years to the day after the first flight. The flight profile was very similar to that of the first flight. The balloon was launched at 8 AM and terminated at 2 AM the following morning, earlier than desired, but required due to its proximity to White Sands Missile Range. The balloon reached a float altitude of 41.8 km, with an ambient air temperature and pressure of −40°C and 2–3 Torr. The payload was successfully recovered with no damage after descending on a parachute and landing 130 miles from the launch facility. Details of the experiment and flight results are discussed in the following sections.

2 Experiment Description

The PICTURE-C experiment is shown in Fig. 1. For flight, the 1500 lb payload is mounted inside the NASA WASP pointing gondola,[9] a two-axis active gimbal mount that provides sub-arcsecond pointing stability. The payload consists of a forward telescope section, the coronagraph instrument (mounted alongside the telescope), and the aft electronics section that houses the experiment flight computer and control electronics for the adaptive optics and thermal control systems. The telescope primary mirror (M1) is a 60 cm off-axis parabola (OAP) and the secondary mirror (M2) is a 14 cm off-axis ellipse (OAE) mounted in a Gregorian configuration.

The flight coronagraph is described in Fig. 2. Additional details regarding the instrument design and laboratory testing can be found in recent publications.[1,2] The coronagraph science bandpass is 20% ($\Delta\lambda/\lambda$) centered at 600 nm (540–660 nm). Inside the coronagraph, the telescope beam is routed through an adaptive optics system consisting of high and low-order wavefront control systems. The LOWFC system[4,12] controls the secondary mirror hexapod, a Physik Instrumente (PI)[13] H-811, and the low-order deformable mirror (LODM), an ALPAO[14] DM97-15 with tip/tilt control. These actuators are driven by two low-order wavefront sensors: a low-speed (40–100 Hz) Shack-Hartmann LOWFS (SH LOWFS) and a high-speed reflective Lyot-stop LOWFS (LLOWFS).[15] The SH LOWFS is used primarily for telescope alignment with the hexapod and to create a diffraction limited image with the LODM. The LLOWFS drives the LODM at high-speed to stabilize the first 23 Zernike wavefront modes while the high-order wavefront control (HOWFC) system is operating. Most importantly, the LLOWFS stabilizes
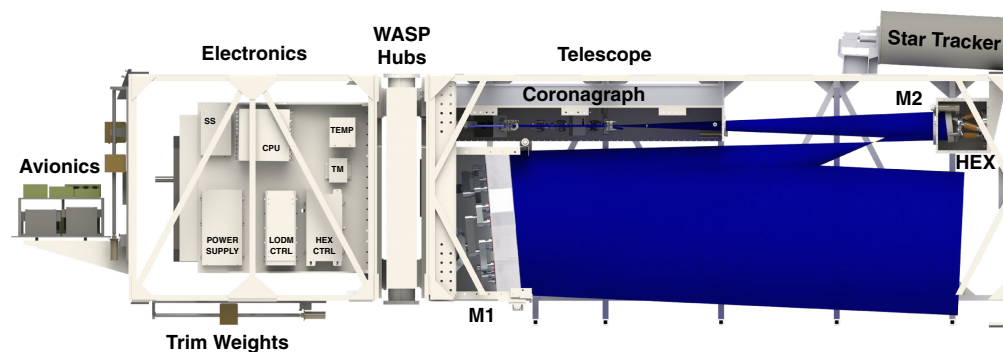
Fig. 1 The PICTURE-C payload consists of two main sections: the forward telescope section and the aft electronics section. The coronagraph instrument is located alongside the 60 cm off-axis telescope. The telescope secondary mirror is positioned actively by a 6-axis hexapod (HEX). The two payload sections are joined by a rigid backplane that mounts the payload to the NASA WASP hubs. WASP is a 2-axis gimbal mount that actively points the science payload to high precision.
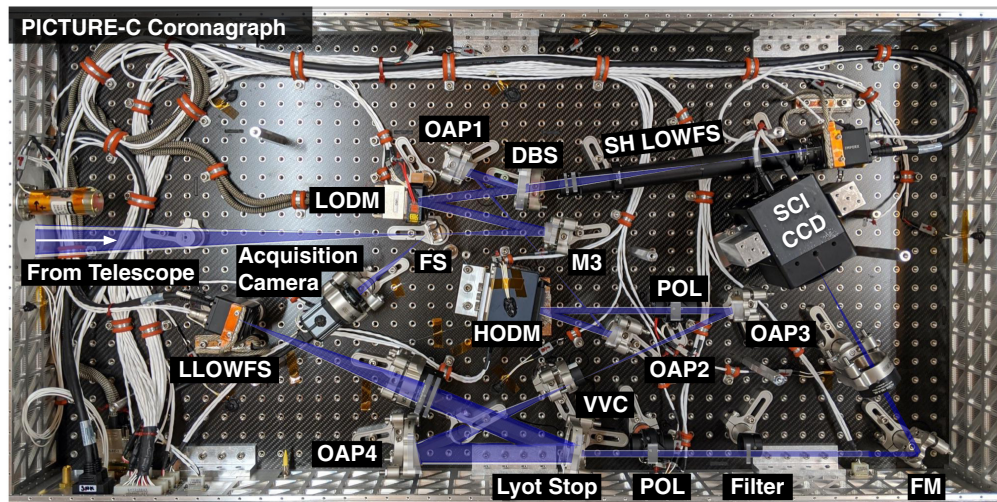
Fig. 2 The PICTURE-C coronagraph is built on a 61 × 122 cm carbon fiber optical bench. Light from the telescope secondary mirror enters from the left. A reflective field stop (FS) with a 20″ (on the sky) hole allows the acquisition camera to view the sky while pointing commands are sent to drop the target star through the hole into the coronagraph. The tertiary mirror (M3) reimages the telescope pupil (primary mirror) to the LODM, which performs low-order wavefront control and pointing stabilization driven by the two LOWFS cameras: a Shack-Hartmann (SH LOWFS) and a reflective Lyot-stop sensor (LLOWFS). The SH LOWFS operates outside the science bandpass (400–540 nm) in a beam transmitted through a shortpass dichroic beamsplitter (DBS). From the LODM, OAP1 and OAP2 reimage the pupil to the HODM, which performs the HOWFC and FPWFS. OAP3 and OAP4 reimage the pupil to the Lyot-stop, with the VVC mask placed at the focus of OAP3. Beyond the Lyot-stop, a fold mirror (FM) and lens focus the image onto the science camera (SCI CCD). The system contains circular polarizers (POL) to improve VVC performance[11] and filters to set the 540–660 nm bandpass.

the residual telescope pointing jitter to keep the star centered on the VVC with milliarcsecond (mas) precision. The SH LOWFS camera is an IMPERX[16] B1020 and the LLOWFS camera is a IMPERX B0620, both operating over the Camera Link interface.

To perform HOWFC, the coronagraph employs a single high-order deformable mirror (HODM) to correct both phase and amplitude errors using EFC[6] and focal plane wavefront sensing (FPWFS).[7] These techniques are used to create a zone of extremely high contrast (dark hole) in one half of the image.[17,18] The microelectromechanical systems (MEMS) HODM is a 952-actuator Boston Micromachines Corporation (BMC) Kilo DM[19] driven by a miniature controller.[20,21] The instrument uses a charge 6 VVC and the dark hole extends from $2.5\,\lambda/D$–$10\,\lambda/D$ ($0.5″$–$2.1″$ on the sky). The science detector is a Finger Lakes Instrumentation (FLI) MLx695 CCD that was cooled to $-30°C$ during the flight using the built-in thermoelectric cooler. The detector has a nominal read noise of 3 e−/px root mean squared (RMS) and dark rate of 0.002 e−/px/s at $-30°C$.

During operations, the experiment is under constant control from the ground with live data streams from all onboard sensors. All experiment data is relayed in real time over a 4 Mbps telemetry link and user commands are sent to the payload through a command uplink system. In this way, the experiment can be operated exactly the same way in flight as it is on the ground.

During the flight, the mission observed 6 different stellar targets and all experiment systems functioned normally. The observation plan for each star followed the nominal sequence:

1. Command WASP to slew to a target.
2. Confirm target visible on instrument acquisition camera.
3. Use WASP and/or secondary mirror hexapod to drop star into the coronagraph entrance aperture.
4. Align secondary mirror using the SH LOWFS.
5. Close LODM loop using the SH LOWFS.
6. Command LODM to center star on VVC.

7. Close LODM loop using the LLOWFS.
8. Run FPWFS and EFC to dig dark hole using the HODM.
9. Transition to observing mode where the HODM is held static and long exposures, up to 60 seconds, are taken.

The experiment was able to reliably progress to step 8 for all targets, but did not achieve the long-term stability required to reach the final observing mode. The mission succeeded in demonstrating two firsts in a near-space environment. The experiment used its HODM to perform FPWFS and EFC to create the first coronagraphic dark hole from a flight platform. Second, the LOWFC system was able to achieve ~1 mas RMS pointing stability over 30 second timescales.

3 Flight Results

PICTURE-C demonstrated the first coronagraphic dark hole from a flight platform in a near-space environment (Fig. 3). Prior to HODM actuation, the raw contrast produced by the VVC alone was $\sim 1 \times 10^{-4}$. The EFC algorithm[6] was then used to further reduce stellar leakage. To implement EFC, pair-wise probe patterns were placed on the HODM to perform FPWFS.[7] A total of 4 probe images were collected and used to estimate the electric field at the focal plane. The field estimation was then multiplied by the inverted HODM response matrix (Jacobian) to calculate a corrective command for the HODM. This response matrix was generated by an optical simulation of the instrument that is built upon the Interactive Data Language (IDL) PROPER[22] library and the VVC model developed under the NASA Strategic Astrophysics Technology (SAT)[23,24] program. The EFC routine was iterated as the D-shaped dark hole region steadily reduced in brightness, creating a higher and higher contrast region of interest to search for dust signals.

As the EFC process was tested throughout the flight, it became clear that while the LOWFC system was maintaining pointing stability at the 1–20 mas level, transient pointing disturbances were occurring regularly and temporarily disturbing the EFC convergence. These transients appeared as large amplitude (~100 mas), very quick (<0.1 seconds) impulsive pointing deflections that were beyond the stabilization authority of the LOWFC system. These rapid transients
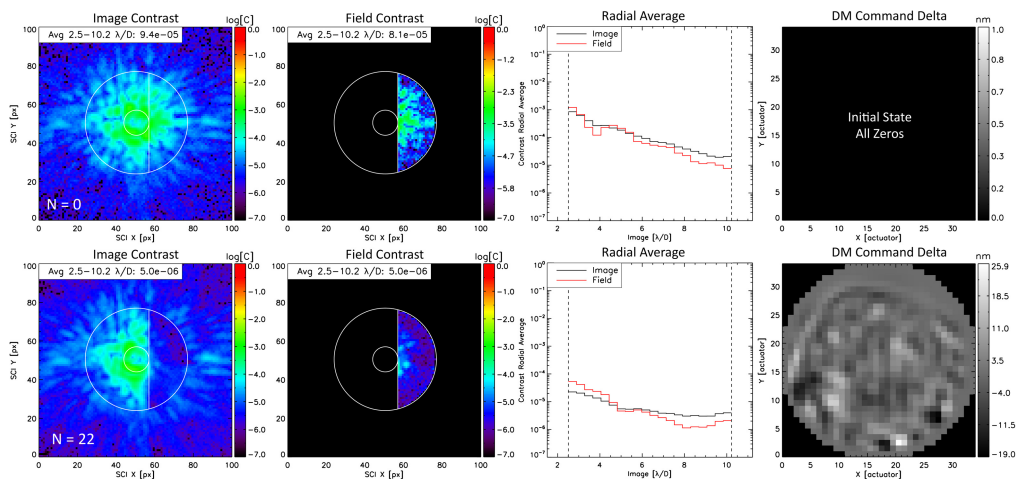
Fig. 3 PICTURE-C in-flight broadband (540–660 nm) high-contrast dark hole generated on stellar target Altair (alf Aql). The initial state is shown along the top row and the final state, after 22 EFC iterations (67 seconds), is shown along the bottom row. *Left to right:* Raw image contrast, field contrast calculated from the measured electric field, radial average of the image and field contrast, DM commands relative to the initial state. The average contrast over the full dark hole (2.5–10.2 λ/D) is shown at the top left corner of each image. The image and field contrast show good agreement overall; the amplitude of the brighter speckles from 3–5 λ/D is slightly over-estimated by the FPWFS solution. To increase the SNR of the final contrast maps, 5 raw images have been averaged together.

would temporarily displace the star from the center of the VVC leading to increased leakage and disturbing the FPWFS routine. In many cases, the inaccurate wavefront estimates caused by these transients would cause the HOWFC system to start diverging, making the dark hole brighter instead of dimmer. These transients occurred on timescales of 1 to 5 minutes and thus prevented the instrument from reaching very deep contrasts, a process that can take 30–60 minutes. During one particularly stable run on the target alf Aql (Altair), which lasted only 67 seconds, the system was able to achieve a raw contrast level of 5×10^{-6} averaged across the 2.5–10 λ/D dark hole (Fig. 3). This was the best contrast achieved during the flight. Pre-flight laboratory measurements were able to reach broadband contrasts of 3×10^{-7}.[1] It was hoped that this level could be improved upon during flight due to likely limitations introduced by the laboratory star simulator. However, telescope pointing transients were the limiting factor.

The raw image contrast shown in Fig. 3 is calculated from individual 0.5 second exposures on the science imaging detector. After background subtraction of detector bias and dark counts, the image is divided by the peak of the unocculted star point spread function (PSF), which was obtained by using the LODM to tilt the star far ($\sim$18 λ/D) from the center of the VVC where the transmission is $\sim$100%. By running the science detector at 1 ms exposures, unsaturated images of the unocculted star could be recorded and used to calibrate the contrast ratio. In cases where the star was too bright and would saturate the detector, HODM sinusoidal test patterns were used to create a calibrated image speckle of known relative brightness. Shown also in Fig. 3 is the field contrast, which is calculated from the electric field estimation obtained through pairwise probe FPWFS images. This is a useful metric for quantifying and separating the coherent leakage (that which is modulated by the HODM probe patterns) from the incoherent background.[25] With good agreement between the image and field contrast, it is clear that the coronagraph was not limited by incoherent leakage sources such as sky background or instrumental scattered light. This observation occurred at approximately 9:20 PM local time, 2 hours after sunset. Quantifying the sky background from residual atmosphere above the balloon will be addressed in a future publication.

As shown in Fig. 4, the pointing stabilization provided by the LOWFC system was not ideal during the dark hole convergence. The system was stable at 16.6 mas in pitch and 11.1 mas in
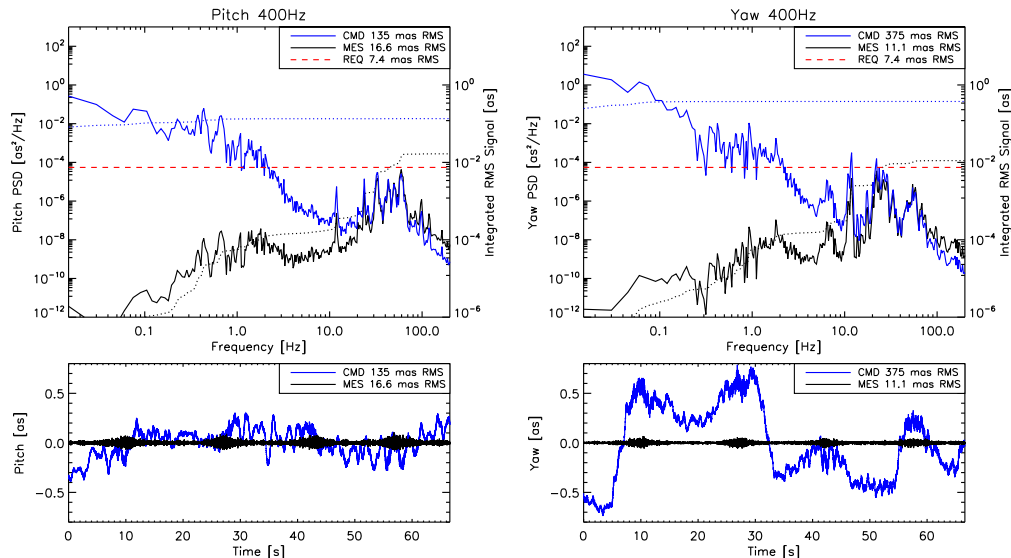
Fig. 4 PICTURE-C pointing stabilization during the 67 second window of dark hole creation shown in Fig. 3. The PSD on top is generated from the time series below. Pitch is shown to the left, yaw to the right. The LOWFC system was running at 400 Hz. The commanded LODM tip/tilt (pitch/yaw) position (CMD, blue) is used as a proxy for the telescope pointing; the mirror tilts to track the telescope. The measured residual error after stabilization is shown in black (MES). RMS values are given in the legends. The dotted lines are the cumulative integral of the PSD, the RMS error, which is referenced to the righthand Y-axis. This integral shows that vibrations above 10 Hz are responsible for pushing the overall stability above the required 7.4 mas RMS (red dashed line).
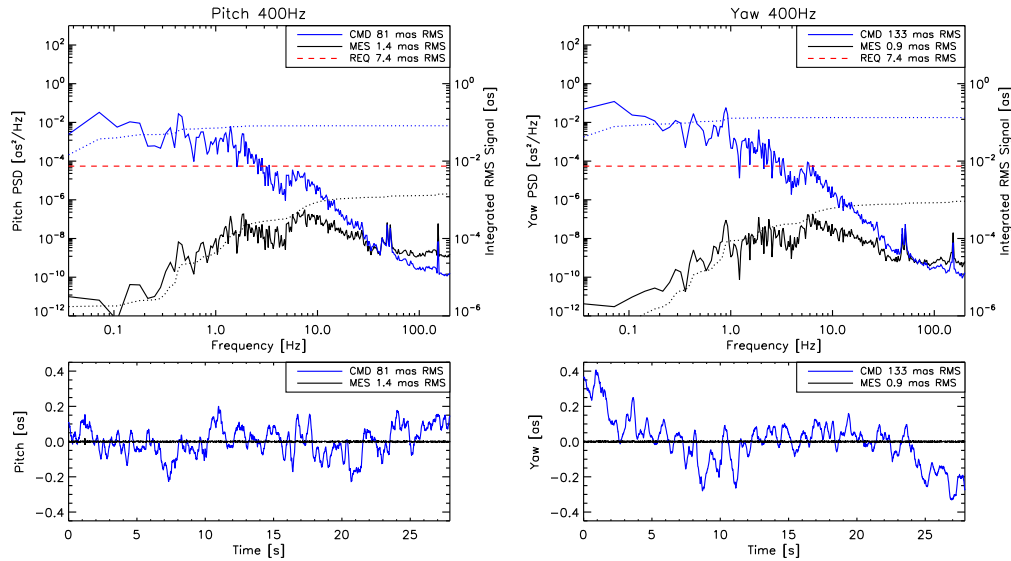
Fig. 5 PICTURE-C ~1 mas pointing stabilization over a 28 second window. This window does not overlap with the window shown in Fig. 4. The PSD on top is generated from the time series below. Pitch is shown to the left, yaw to the right. The LOWFC system was running at 400 Hz. The commanded LODM tip/tilt (pitch/yaw) position (CMD, blue) is used as a proxy for the telescope pointing; the mirror tilts to track the telescope. The measured residual error after stabilization is shown in black (MES). RMS values are given in the legends. The dotted lines are the cumulative integral of the PSD, the RMS error, which is referenced to the righthand Y-axis. Reduced high-frequency vibrations (compared with Fig. 4) allowed the stability to remain well below the required 7.4 mas RMS (red dashed line).

yaw (RMS values). A large amount of high-frequency (10–100 Hz) vibration is present in the power spectral density (PSD) curve, as well as a periodic packet of vibration at ~17 second intervals. The sources of these vibrations are still being investigated by the experiment and WASP teams. It is unclear if they were true mechanical vibrations or induced oscillations of the LOWFC system. These vibrations were not persistent throughout the flight. During a 28 second window earlier in the flight, the pointing environment was quiet enough to achieve 1.4 mas stabilization in pitch and 0.9 mas in yaw (Fig. 5). This stability satisfies the mission pointing requirement of 7.4 mas RMS in each axis, which is defined (along with the first 23 low-order Zernike modes) to allow at most 1×10^{-8} contrast leakage due to low-order residuals.

As the flight progressed past sunset (7 PM local time), the instrument started to experience large-amplitude (~$10''$) pointing drift oscillations on timescales of 1 to 2 minutes. These drifts were fairly constant and beyond the correction range of the LODM and thus prevented further operation of the HOWFC system. The pointing drift was measured only by the coronagraph LOWFS and not by the WASP system. During the flight, we hypothesized that the thermal shock of sunset on the payload was driving mechanical deformation of the telescope truss and moving the secondary mirror, creating a perceived pointing drift. Post-flight analysis has revealed, however, that the perceived drift was caused by a misalignment between the telescope and WASP pointing axes (boresights). As the telescope swings beneath the balloon, the sky rotates slightly in the WASP frame of reference about the pointing center, which is defined by the star tracker camera (Fig. 1). If the telescope and WASP boresights are misaligned, this roll maps into perceived pitch and yaw in the instrument. Analysis of the flight pointing data shows pointing drifts that are highly correlated with telescope roll – and not with telescope truss temperature. A boresight misalignment of less than 5 arcmin can explain all of the observed drifts. The telescope and instrument have no absolute boresight reference. It is likely that repeated re-alignment of the secondary mirror and slow thermal drift of the truss over many hours introduced a boresight offset that was imperceptible to the experiment team and led to the observed pointing drift.

4 Discussion

The second flight of PICTURE-C has demonstrated the first coronagraphic dark hole in a near-space environment and ∼1 mas pointing stability. Performance of the HOWFC system was limited both by transient pointing disturbances and large-amplitude pointing drifts owing to telescope and WASP misalignment. While image post-processing has been shown to improve the effective contrast of coronagraph observations,[26–28] the paucity of high-contrast images from PICTURE-C would likely not provide enough information for accurate speckle reduction. Likewise, dust detection around Altair is unlikely due to the lack of deep exposures at high contrast and lack of observable dust in the system. Altair shows no mid or far infrared excess[29,30] that would indicate warm dust detectable by PICTURE-C. The star was chosen as a dust-free calibration target to provide a PSF reference to enable reference star differential imaging (RDI)[31] on the science target alf Lyr (Vega).

The contrast performance achieved during this flight is roughly a factor of 1000 times worse than the current state-of-the-art in laboratory VVC testing.[25] This remarkable difference serves to highlight the difficulty of operating a high-contrast coronagraph in a remote flight environment. PICTURE-C operates in partial atmosphere at −40°C on a moving platform in Earth's gravity with pointing stability 10–100 times worse than what has been demonstrated in space. Our current challenges are still dominated by observatory stability and low-order wavefront control. These concerns are of paramount interest to future large space telescopes as well.[32]

PICTURE-C and its successor, PICTURE-D, will continue to drive the improvement of the WASP platform, much in the same way that the original PICTURE sounding rocket drove innovations in the rocket attitude control system that enabled 5 mas pointing stability in space.[33] Work has begun to develop mitigation strategies and engineering solutions to remedy both pointing issues that hindered EFC convergence. While the ∼1 mas image stabilization proves that pointing stability equivalent to the James Webb Space Telescope (JWST)[34] is possible from the highly dynamic environment of a sub-orbital balloon, a great deal of work is required to achieve this level of performance over hour-long observation timescales. Simple software updates could greatly improve dark hole convergence by implementing LOWFC transient detection that would allow the HOWFC system to avoid recording data during pointing disturbances. The WASP team has already begun an overhaul of their pointing motors to reduce vibration and structural improvements are being investigated to reduce transients likely caused by creaking of the gondola suspension cables. The goal for future flights would be to limit the transient occurrence frequency to timescales much greater than 60 seconds, which is the planned maximum exposure time for the science images, and to reduce high frequency vibration from 10–100 Hz by roughly an order of magnitude to allow the LOWFC system to maintain the 7.4 mas RMS stability requirement over 1–2 hour timescales. To address boresight misalignment and drift, a communication interface will be established to send live pointing updates from the experiment LOWFS to WASP. Enabling this link will allow WASP to guide on the instrument boresight and completely eliminate the perceived drift. For future flights, the experiment will also incorporate a pupil locating camera that will provide an absolute reference for the telescope boresight. This camera will be used to break the degeneracy between the secondary mirror alignment and the telescope pointing; a positive tilt of M2 can be compensated by a negative tilt of the telescope. This would result in a displacement of the pupil on M2 and further downstream on the pupil camera where it can be sensed and corrected. This type of misalignment would also introduce wavefront error that could be sensed by the SH LOWFS and used to correct the alignment.

The goal of the PICTURE family of sub-orbital experiments[2,33,35] since their inception in 2005 has been to develop necessary technologies and operations concepts to help pave the way for direct imaging of exoplanets with future space missions such as the Habitable Worlds Observatory (HWO) prioritized by the Astro 2020 Decadal Survey.[36] This effort has been funded under the NASA Astrophysics Research and Analysis (APRA) program for an additional 5 years and will transition into PICTURE-D with flights in 2024 and 2026. The goal of these flights is to continue technology maturation through the incorporation of new deformable mirror electronics and vortex coronagraph technologies, and also to begin full-scale science operations by capturing images of several nearby debris disk systems. The new mission will incorporate multi-star wavefront control (MSWC)[37–39] for capturing high-contrast images around binary stars and a

double-grating vector vortex coronagraph (dgVVC)[40] which will enable polarimetry measurements of debris disks.

Acknowledgments

References

1. C. B. Mendillo et al., "The PICTURE-C exoplanetary imaging balloon mission: laboratory coronagraph demonstrations of high-contrast imaging and low-order wavefront control," *Proc. SPIE* **12180**, 1218022 (2022).
2. C. B. Mendillo et al., "The PICTURE-C exoplanetary imaging balloon mission: first flight results and second flight preparation," *Proc. SPIE* **11823**, 118230X (2021).
3. C. B. Mendillo et al., "Optical tolerances for the PICTURE-C mission: error budget for electric field conjugation, beam walk, surface scatter, and polarization aberration," *Proc. SPIE* **10400**, 1040010 (2017).
4. C. B. Mendillo et al., "The low-order wavefront sensor for the PICTURE-C mission," *Proc. SPIE* **9605**, 19 (2015).
5. T. Cook et al., "Planetary imaging concept testbed using a recoverable experiment-coronagraph (PICTURE-C)," *J. Astron. Telesc. Instrum. Syst.* **1**, 044001 (2015).
6. A. Give'on et al., "Broadband wavefront correction algorithm for high-contrast imaging systems," *Proc. SPIE* **6691**, 66910A (2007).
7. A. Give'on, B. D. Kern, and S. Shaklan, "Pair-wise, deformable mirror, image plane-based diversity electric field estimation for high contrast coronagraphy," *Proc. SPIE* **8151**, 815110 (2011).
8. C. B. Mendillo et al., "Polarization aberration analysis for the PICTURE-C exoplanetary coronagraph," *J. Astron. Telesc. Instrum. Syst.* **5**, 025003 (2019).
9. D. W. Stuchlik and R. J. Lanzi, "The NASA wallops arc-second pointer (WASP) system for precision pointing of scientific balloon instruments and telescopes," 20180002870, NASA Technical Reports Server (2017).
10. D. Mawet et al., "The vector vortex coronagraph: sensitivity to central obscuration, low-order aberrations, chromaticism, and polarization," *Proc. SPIE* **7739**, 14 (2010).
11. D. Mawet et al., "Recent results of the second generation of vector vortex coronagraphs on the high-contrast imaging testbed at JPL," *Proc. SPIE* **8151**, 81511D (2011).
12. C. B. Mendillo et al., "The PICTURE-C exoplanetary direct imaging balloon mission: first flight preparation," *Proc. SPIE* **11117**, 101–111 (2019).
13. Physik Instrumente (PI) website, www.physikinstrumente.com.
14. ALPAO website, www.alpao.com.
15. G. Singh et al., "Lyot-based low order wavefront sensor for phase-mask coronagraphs: principle, simulations and laboratory experiments," *PASP* **126**, 586–594 (2014).
16. IMPERX website, www.imperx.com.
17. F. Malbet, J. W. Yu, and M. Shao, "High-dynamic-range imaging using a deformable mirror for space coronography," *PASP* **107**, 386 (1995).
18. L. Pueyo et al., "Optimal dark hole generation via two deformable mirrors with stroke minimization," *Appl. Opt.* **48**, 6296–6312 (2009).
19. Boston Micromachines website, www.bostonmicromachines.com.
20. E. Bendek et al., "Development of a miniaturized deformable mirror controller," *Proc. SPIE* **9909**, 990984 (2016).
21. E. A. Bendek et al., "Microelectromechanical deformable mirror development for high-contrast imaging, part 1: miniaturized, flight-capable control electronics," *J. Astron. Telesc. Instrum. Syst.* **6**(4), 045001 (2020).

22. J. E. Krist, "Proper: an optical propagation library for IDL," *Proc. SPIE* **6675**, 66750P (2007).
23. NASA SAT website, https://exoplanets.nasa.gov/exep/technology/TDEM-awards/.
24. J. E. Krist et al., "End-to-end simulations of different coronagraphic techniques," *Proc. SPIE* **7440**, 16 (2009).
25. G. J. Ruane et al., "Broadband vector vortex coronagraph testing at NASA's high contrast imaging testbed facility," *Proc. SPIE* **12180**, 1218024 (2022).
26. M. Ygouf et al., "Data processing and algorithm development for the WFIRST coronagraph: comparison of RDI and ADI strategies and impact of spatial sampling on post-processing," *Proc. SPIE* **9904**, 99045M (2016).
27. M. Ygouf et al., "Data post-processing and algorithm development for the wfirst coronagraph: Fy16 interim report," (2016).
28. M. Ygouf et al., "Roman coronagraph instrument post processing report - os9 hlc distribution" (2021).
29. S. Ertel et al., "The HOSTS survey for exozodiacal dust: Observational results from the complete survey," *Astron. J.* **159**, 177 (2020).
30. B. Mennesson et al., "Constraining the exozodiacal luminosity function of main-sequence stars: complete results from the Keck Nuller mid-infrared surveys," *ApJ* **797**, 119 (2014).
31. G. Ruane et al., "Reference star differential imaging of close-in companions and circumstellar disks with the nirc2 vortex coronagraph at the W. M. Keck observatory," *ApJ* **157**, 118 (2019).
32. R. Juanola-Parramon et al., "Modeling and performance analysis of the LUVOIR coronagraph instrument," *J. Astron. Telesc. Instrum. Syst.* **8**(3), 034001 (2022).
33. C. B. Mendillo et al., "Flight demonstration of a milliarcsecond pointing system for direct exoplanet imaging," *Appl. Opt.* **51**, 7069–7079 (2012).
34. J. Rigby et al., "The science performance of JWST as characterized in commissioning," *Publ. Astron. Soc. Pacific* **135**(1046), 31 (2022).
35. E. S. Douglas et al., "Wavefront sensing in space: flight demonstration ii of the PICTURE sounding rocket payload," *J. Astron. Telesc. Instrum. Syst.* **4**, 019003 (2018).
36. National Academies of Sciences, Engineering, and Medicine, *Pathways to Discovery in Astronomy and Astrophysics for the 2020s*, The National Academies Press, Washington, DC (2021). https://doi.org/10.17226/26141
37. S. Thomas, R. Belikov, and E. Bendek, "Techniques for high-contrast imaging in multi-star systems. I. Super-nyquist wavefront control," *Astrophys. J.* **810**, 81 (2015).
38. D. Sirbu et al., "Techniques for high-contrast imaging in multi-star systems. II. Multi-star wavefront control," *Astrophys. J.* **849**, 142 (2017).
39. R. Belikov et al., "High-contrast imaging in multi-star systems: progress in technology development and lab results," *Proc. SPIE* **10400**, 104000W (2017).
40. D. S. Doelman et al., "Minimizing the polarization leakage of geometric-phase coronagraphs with multiple grating pattern combinations," *Publ. Astron. Soc. Pacific* **132**, 045002 (2020).

Christopher B. Mendillo is a research professor at UMass Lowell. He received his PhD in astronomy from Boston University in 2013 and his BSc degree in physics from Brown University in 2005.

Kuravi Hewawasam is a post-doctoral research fellow at UMass Lowell. He received his BSc degree in physics from the University of Colombo, Sri Lanka, in 2007 and his MS degree in physics from University of Minnesota, Duluth, in 2012.

Jason Martel is a mechanical engineer at UMass Lowell. He received his BSc degree in mechanical engineering from Boston University in 2010.

Thaddeus Potter is a PhD candidate at UMass Lowell. He received his BSc degree in chemistry and physics from Stetson University in 2017.

Timothy A. Cook is a professor of physics at UMass Lowell. He received his PhD in astrophysics from the University of Colorado in 1991 and his BA degree in physics from Johns Hopkins University in 1985.

Supriya Chakrabarti is a professor of physics at UMass Lowell. He is the P.I. of the PICTURE-C mission. He received his MS and PhD degrees from the University of California, Berkeley, in 1980 and 1982, respectively, and his BE degree from the University of Calcutta, Calcutta, India, in 1975.